1 **Microtubules and Gαo-signaling independently regulate the preferential**

2 **secretion of newly synthesized insulin granules in pancreatic islet β cells**

3

4 Ruiying Hu[1], Xiaodong Zhu[1, 2], Mingyang Yuan[1], Kung-Hsien Ho[1], Irina Kaverina[1, *],

5 and Guoqiang Gu[1,*,#]

6

7 [1]Department of Cell and Developmental Biology, The Program of Developmental

8 Biology and the Vanderbilt Center for Stem Cell Biology, Vanderbilt University,

9 Nashville, TN

10 [2]Curent affiliation: Department of Medicine and Molecular Physiology and

11 Biophysics, Vanderbilt University, Nashville, TN

12 *Corresponding authors: Guoqiang.Gu@vanderbilt.edu (615-936-3634)

13   Irina.Kaverina@vanderbilt.edu (615-936-5568)

14 #: lead contact.

15 OCRID for Guoqiang Gu: 0000-0003-0772-9139

16

17

18

19 **Abstract**

20   For sustainable function, each pancreatic islet β cell maintains thousands of

21 insulin granules (IGs) at all times. Glucose stimulation induces the secretion of a

22 small portion of these IGs and simultaneously triggers IG biosynthesis to sustain this

23 stock. The failure of these processes, often induced by sustained high-insulin output,

24 results in type 2 diabetes. Intriguingly, newly synthesized IGs are more likely

25 secreted during glucose-stimulated insulin secretion. The older IGs tend to lose

26 releasability and be degraded, which represents a futile metabolic load that can

27 sensitize β cells to workload-induced dysfunction and even death. Here, we examine

28 the factor(s) that allows the preferential secretion of younger IGs. We show that β

29 cells without either microtubules (MTs) or Gαo signaling secrete a bigger portion of

30 older IGs, which is associated with increased IG docking on plasma membrane. Yet

31 Gαo inactivation does not alter the β-cell MT network. These findings suggest that

32 Gαo and MT regulate the preferential release of newer IGs via parallel pathways and

33 provide two potential models to further explore the underlying mechanisms and

34 physiological significance of this regulation in functional β cells.

35

36

Introduction

37

38   In response to postprandial blood-glucose increase, pancreatic islet β cells

39   secrete insulin to promote glucose usage and storage in peripheral tissues (the liver,

40   fat, and skeletal muscle), ensuring blood-glucose homeostasis. The collective β-cell

41   dysfunction, loss-of identity, or death (a.k.a. β-cell failure) results in inadequate

42   insulin secretion (1-3). This leads to type 2 diabetes (T2D), featured by sustained

43   high blood-glucose levels and deregulated lipid metabolism that damage multiple

44   tissues (4). In contrast, excessive insulin secretion, caused by cancerous β-cell

45   proliferation (5) or deregulated secretion (6, 7), results in hyperinsulinemic

46   hypoglycemia that leads to comatose or even death.

47

48   To control insulin secretion, β cells precisely regulate insulin biosynthesis,

49   storage, transport, and secretion (8). Each β cell contains around 10,000 IGs (9).

50   According to the physical location of and response to stimulus, these IGs have been

51   traditionally classified into two pools: the readily releasable pool (RRP) and reserve

52   pool (RP) (10). The former refers to a small group of IGs (<5%) that are docked onto

53   the plasma membrane (PM) (11). These IGs were immediately released upon

54   stimulation and largely contribute to the first phase of insulin secretion (11). In

55   dysfunctional islets from T2D patients, β cells lack this IG pool, so that they cannot

56   quickly secrete insulin in response to glucose stimulation within the first few

57   minutes, i. e., the first phase (12). The RRP is absent in newly differentiated

58   immature β cells as well, likely depleted by high levels of basal secretion (13).

59

60 The RP contains the majority of IGs in β cells, which are usually located away

61 from the PM. These vesicles need transport to the PM for docking and priming to be

62 released. To this end, high glucose, besides triggering glucose-stimulated insulin

63 secretion (GSIS) and new IG biosynthesis, induces the transport and conversion of

64 some IGs from RP to replenish the RRP (10, 14-17). These inter-connected

65 responses allow β cells to maintain sustained or pulsatile GSIS under continuous or

66 pulses of glucose stimulation, a property that is necessary for long-term β-cell

67 function.

68

69 Intriguingly, not all IGs in the RP are alike and are able to be mobilized to the

70 RRP. Several studies, using pulsed radio-labeling or fluorescent-protein tagging of

71 insulin, have shown that newly synthesized IGs are more likely released upon

72 stimulation (18-23). Aged IGs will become non-functional and degrade via

73 proteolysis (24, 25). This degradation ensures long-term β-cell function by

74 removing the non-responsive IGs. It also presents additional metabolic load due to

75 the futile biosynthesis of these IGs, which contributes to the high β-cell stress and

76 reduced cell proliferation/function (26-29). Thus, investigating how β cells

77 preferentially secrete newly synthesized IGs can lead to ways to enhance insulin

78 output while avoiding insulin biosynthesis-induced dysfunction.

79

80 A feature that potentially contributes to the preferential release of new IGs is

81 their transportability via the microtubule (MT) network. In an elegant study of

82 temporally-marked IGs, Hoboth and colleagues showed that IGs can display three

4

83   types of glucose-modulated and MT-dependent mobility: highly dynamic, restricted,

84   and nearly immobile states. High glucose can expedite this motion, with the young

85   IGs being more responsive to glucose, and older ones less sensitive and more likely

86   found in the lysosome (30). These findings support a model that old IGs tend to lose

87   MT-dependent transportability, preventing their movement to the PM and reducing

88   their chance of docking/release.

89

90   MTs are cytoskeletal biopolymers that act as tracks for vesicular transport

91   using the kinesin and dynein motor proteins (31, 32). In many cell types, MTs

92   originate from the centrosome to form a radial array, with their plus ends oriented

93   toward the cell periphery. Henceforth, kinesin- or dynein-mediated transport

94   mediates the bulk flow of cargo toward the cell periphery or interior, respectively

95   (33). In contrast, most of the β-cell MTs originate from organizing centers in the

96   Golgi and form a non-directional meshwork (34, 35). This network is essential for

97   quick/long-range IG movement but is ill-suited for bulk directional cargo transport

98   (34-39). Disrupting these MTs acutely enhances GSIS (34, 35, 40), while stabilizing

99   the MTs represses secretion (34, 35, 41). A model that is supported by these

100   findings is that β-cell MTs allow active IG-movement between cell interior and cell

101   periphery; however, MTs also compete with the PM for IG binding to acutely reduce

102   the RRP. In the absence of MTs, the overall long-range IG transport is reduced (35,

103   38, 39). Yet the non-MT-dependent IG movement, within a brief period of time, is

104   sufficient for a portion of IGs to move to the PM for docking and regulated release

105   (35). Thus, regulating the dynamics and density of MTs will likely influence the

106   releasability of young versus old IGs, because the new IGs will lose their advantage

107   of being moved to cell periphery when MT-aided transport is reduced.

108

109   In addition to transport, IG docking on the PM is another limiting step for

110   insulin secretion (15, 17, 42, 43). In this case, vesicular and PM proteins form a

111   SNARE complex via the association between Synaptobrevins, Syntaxins, SNAP23/25,

112   Munc18, Rim, and others (44). This complex brings the vesicles close to the PM. The

113   presence of Ca^{2+}, via a family of Ca^{2+} sensors such as Synaptotagmins (Syts) (13, 45,

114   46) and/or Doc2B (47-49), further modulate the conformation of the SNARE-

115   complex to enable vesicular/PM fusion (50). Thus, mutations in several of these

116   SNARE components were found to deregulate IG docking and secretion, and

117   underscore essential roles of docking in GSIS (17, 43, 51-54).

118

119   An intriguing signaling molecule that can potentially regulate both IG docking

120   and MT dynamics is inhibitory G protein Gαo. Like all other Gα subunits, Gαo

121   signaling toggles between on- and off-state by dissociating/associating with Gβγ

122   dimers in response to the activation of G-protein coupled receptors (55). Unlike

123   other inhibitory Gα (Gαi1, Gαi2, Gαi3, and Gαz), Gαo activation does not inhibit

124   adenylyl cyclases in several cell types including islet β cells (15, 56), but repressing

125   GSIS by reducing IG docking (15). Intriguingly, Gαo at high levels, together with

126   other inhibitory Gα subunits, was shown to promote MT disassembly by Gα-MT

127   association (57, 58). Here, we explore the hypothesis that Gαo may regulate IG

128   transport/docking through the MT network, which consequently control the

129   probability of IG secretion in young and aged IG pools.

130

131   **Results and discussion**

132

133   **The β-cell MTs are dispensable for overall IG-distribution to cell periphery**

134   We have previously shown that the MT network in β cells, although essential

135   for sustained secretory function (40), acutely represses GSIS (35, 40, 59). Based on

136   Total Internal Reflection Fluorescence Microscopy (TIRFM)-observation of MT-

137   dependent IG movement near cell membrane (<200 nm away from the PM), we

138   postulated that a role of the MT network in β cells is to pull IGs away from the PM

139   besides acting as tracks for long-distance IG movement (34, 35). Here, we

140   corroborated this hypothesis by first examining the overall distribution of IGs in β

141   cells with or without MTs.

142

143   Isolated islets were stained for insulin immunofluorescence (IF) and confocal

144   microscopy after incubation in 10 μg/ml Nocodazole (NOC) for 12 hours, a

145   condition that effectively destabilize MTs (Figure 1A, B). We then examined the

146   insulin levels at different areas of β cells, starting from one spot of β-cell membrane

147   to another on the opposite side of cell membrane (see white lines in Figure 1C). At

148   both non-stimulating 2.8 mM glucose (G2.8) and stimulating G20, there were

149   significant reductions in total IG levels when cells were treated with NOC (Figure

150   1D), with $p = 0.0015$ and $p < 0.0001$ (ANOVA), respectively. We observed particularly

151 high IG reduction in the center of cells in islets treated with G20 and NOC, when the

152 overall IG was quantified (Figure 1D) or when the relative distribution of IGs (i.e.,

153 the % of IGs distributed at each spot of β cells) were examined (Figure 1E). These

154 findings are consistent with our conclusion that MTs are dispensable for the

155 movement of IGs to cell periphery, likely achieved by slow-but-detectable random

156 IG movement or MT-independent transport (35).

157

158 **Figure 1. MTs are dispensable for the allocation of IGs near the β-cell**
159 **periphery.** (A-C) IF-assays of IG distribution in intact islets treated with [2.8 mM
160 glucose (G2.8) + DMSO] (column 1), (G2.8 + NOC) (column 2), (G20 + DMSO)
161 (column 3), and (G20 + NOC) (column 4). Images shown in (A) are maxi-projections
162 of Z-stacked optical sections, showing co-staining of insulin (red), E-cadherin (E-
163 Cad, blue), and α-tubulin (green). (B, C) high-magnification images showing α-
164 tubulin (B) or (insulin + Ecad, C) IF signals in boxed areas of (A). Broken white
165 circles highlight quantified β cells. Panel (B) images verify the absence of detectable
166 MT filaments with NOC-treatment. Panel (C) shows the way of quantifying insulin
167 distribution – with a line-scan along the white line drawn across each β cell. (D) IF
168 intensity profile of insulin along the long axis of β-cells from confocal images. (E)
169 Another way to show the insulin-distribution patterns with/without MT disruption,
170 with the % of insulin detected at different locations in β cells along the long axis. P
171 values marked in both (D) and (E) were calculated with two-tailed type II t-tests
172 from the data of (DMSO + G20) and (NOC + G20) groups.
173
174
175

176 **The β-cell MT inhibits IG docking on PM**

177 We next examined the number of docked IGs via TEM in the absence of MTs,

178 focusing on vesicles <10 nm away from the PM, a resolution that cannot be achieved

179 by TIRFM or confocal microscopy (Figure 2A, B). MT-depolymerization significantly

180 increased the number of IGs docked onto the β-cell PM at basal glucose (Figure 2C).

181 In contrast, there is a significant decrease in the density of IGs in β cells without MTs

182 (Figure 2D-F), consistent with the requirement of MTs for new IG biosynthesis (40).

8

183   Similarly, the increased IG docking was observed in the absence of MTs under high

184   glucose conditions (Figure 2G-I), despite significant degranulation with or without

185   MTs under high glucose (Figure 2J. Compare with Figure 2F).

186   **Figure 2. TEM imaging showing the inhibitory effects of MTs on IG-docking in β**
187   **cells.** Islets were isolated from wild-type (WT) adult ICR mice and were treated
188   with DMSO or 10 μg/ml NOC for ~12 hour at 5.6 or 20 mM glucose. TEM was then
189   used to examine the locations and density of IGs. (A-C) TEM images and
190   quantification of docked IGs from DMSO- and NOC-treated islets in the presence of
191   5.6 mM glucose. (D-F). Images and quantification of IG density in microscopic fields
192   used in (A-C). (G-J) Images and IG quantification as in (A-F), except 20 mM glucose
193   was used. Scales in (D, E, G, H) are the same, labeled in panel (H). In (C), (F), (I), and
194   (J), mean + SEM were presented. In all panels, "n" indicates the number of
195   microscopic fields (with 3-4 different β cells included in each field) counted. P,
196   results from two-tailed type II t-test.
197
198   These results are consistent with a model that MTs compete with the PM for

199   IG binding. Specifically, IGs likely associate with MTs via vesicle-bound motor

200   proteins. This allows the MT-dependent IG-transport from the site of biogenesis, the

201   trans-Golgi network that usually localizes in interior of cells, to close-to the PM (34,

202   36-39, 60, 61). However, the β-cell MTs have no obvious directionality. Thus, the

203   MTs can also pull IGs away from the PM to prevent IG docking and to reduce the

204   RRP, supported by both experimental results (17, 35) and mathematical modeling

205   (34). When MTs are destabilized near the PM, e.g., in the presence of high glucose,

206   the IGs can lose MT contact and be available for docking/secretion. Consequently,

207   IGs with preferential binding with MTs, especially those newly synthesized (30), are

208   more likely transported to the cell periphery for docking and release (59). The

209   older vesicles, less likely transported due to their attenuated MT-association, will

210   eventually be degraded.

211

212   The above model predicts that when the MT network is disrupted, the fast IG

213   movement will be abolished (30, 36). Yet vesicle movement [slowed but still

214   detectable in the absence of MTs (35)] via free-diffusion or actin-assisted transport

215   is probably sufficient for a portion of IGs to move to underneath the PM for docking

216   and regulated secretion (58, 62). In this setting, older IGs can be mobilized to allow

217   enhanced secretion without new IG biosynthesis. In addition, the newly synthesized

218   IGs with superior MT-dependent transportability will lose the advantage of being

219   moved to underneath the PM (30). In other words, the absence of MTs could

220   normalize the probability of secretion for both new and older IGs, which we

221   experimentally evaluated next.

222

223   **Disrupting the MTs allows increased secretion of older IGs from β cells**

224   To test if MT-disruption induces increased secretion of old IGs, GSIS was

225   carried out in the absence of protein synthesis and MTs. Islets were incubated in the

226   presence of 10 μM cycloheximide (CHX) for three-hours, a condition that can

227   effectively (>95%) inhibit protein biosynthesis in islets (63). Treated islets were

228   then incubated with 10 μg/ml NOC for one more hour to disrupt islet-cell MTs

229   (Figure 3A-D), followed by GSIS assays. Because newly synthesized insulin become

230   secretable within two-hours (64), we expect this treatment to reduce newly

231   produced secretable IGs. The lack of protein biosynthesis results in a significant

232   reduction in GSIS in β cells with functional MT (i.e., without NOC-treatment) (p=

233   0.02, Figure 3E) as expected (63). Yet this lack of protein synthesis did not eliminate

234   the MT-destabilization-enhanced GSIS (Figure 3E).

235

236 **Figure 3. The absence of MTs promotes secretion of aged IGs.** (A-D) The
237 effective MT-disruption in islet β cells with NOC. Glu-tubulin was stained (A, B) to
238 verify the effective disruption of MTs by NOC, with β cells identified by insulin
239 staining (C, D, corresponding to the fields in A, B, respectively). Arrows in (A, B),
240 primary cilia. Scale bar = 10 μm. (E) GSIS from islets treated with combination of 10
241 μg/ml NOC and 10 μM CHX. (F) The relative amount of radioactive insulin that are
242 secreted (count/pg insulin) in control and NOC-treated islets, immediately following
243 a 12-hour radio-labeling process. Presented in (E) and (F) were (mean + SEM). The
244 P values presented are from two-tailed type II t-test. "n", the number of independent
245 assays.
246

247   We next compared the secretion-probability of old and new IGs directly.

248 Isolated islets were incubated overnight with 3H-labeled leucine/isoleucine and

249 used in GSIS assays with or without NOC treatment. MT-disruption (in the presence

250 of NOC) induced a significant increase in the proportion of older IGs being released

251 (Figure 3F). These data support our model that the dense MT network in β cells

252 traps older IGs. Without MTs, a bigger portion of older IGs will be made available for

253 GSIS, leading us to explore the mechanisms that regulate both the MT networks and

254 older vesicle docking/secretion in β cells. Note that the half-life of IGs in β cells was

255 reported to be 3 – 5 days, we therefore consider IGs synthesized within the 12-hour

256 window immediately before secretion assay as new IGs (25). This time-period

257 allows sufficient amount of 3H-leucine/isoleucine incorporation in insulin for

258 quantification.

259

260 **Gαo inactivation preferentially increases the secretion-probability of old IGs**

261   The increased vesicle docking in MT-destabilized β cells is similar to what we

262 have observed in the pancreatic specific *Gαo* mutant (*Gαo$^{F/F}$; Pdx1^{Cre}*) mouse β cells

11

263   (15). Based on the published findings that trimeric G proteins can regulate MT

264   dynamics (57, 65, 66), we explored the possibility that Gαo regulates IG secretion

265   through MTs. We first tested if Gαo inactivation would impact the preferential

266   secretion of newer IGs. As in the case of MT-destabilization, the $Gαo^{F/F}$; $Pdx1^{Cre}$ β

267   cells, wherein $Gαo$ is efficiently inactivated in β cells (Figure 4A-D), secrete a larger

268   portion of older vesicles under high-glucose stimulation (Figure 4E).

269
270   **Fig. 4. Gαo and MT regulate IG secretion via parallel pathways.** (A-D)
271   Immunoassays showing the complete Gαo inactivation in $Gαo^{F/F}$; $Pdx1^{Cre}$ islet cells.
272   Note that Cre-mediated $Gαo^{F}$ deletion will yield a mRNA that translates a short N-
273   terminal Gαo peptide, recognized by the antibody (red) but has no detectable
274   biological effect (15). Full length funtional Gαo is membrane-bound, while the N-
275   terminal fragment is cytoplasmic, allowing for ready verification of $Pdx1^{Cre}$-
276   mediated $Gαo$ inactivation in insulin+ (green) cells. DAPI (blue) stained for nuclei.
277   Scale bar, 20 μm. (E) The levels of ^{3}H-labeling in secreted insulin from control and
278     $Gαo^{F/F}$; $Pdx1^{Cre}$ β cells. (F) Insulin secretion results in $Gαo^{F/F}$; $Pdx1^{Cre}$ islets, with or
279   without NOC-treatment, induced by basal G2.8, stimulating G20, and [(A, B) G20 +
280   K25 (25 mM KCl)]. Presented data in E and F are (mean + SEM). P values, results
281   from two-tailed type II t-test.
282

283   **Gαo inactivation and MT disassembly independently regulate GSIS**

284   We then tested if the increased GSIS in $Gαo^{F/F}$; $Pdx1^{Cre}$ and MT-disrupted β

285   cells depends on mobilizing a same pool of IGs. If so, we expect that MT disassembly

286   in $Gαo^{F/F}$; $Pdx1^{Cre}$ β cells will not further increase GSIS. In contrast, treating Gαo$^{-/-}$ β

287   cells with NOC induced an additional enhancement in GSIS (Figure 4F). Thus,

288   different pools of IGs were mobilized/secreted in response to Gαo inactivation and

289   MT disassembly, implying that Gαo does not directly regulate MTs in β cells.

290

291   **Gαo does not regulate MTs in β cells.**

292   We finally compared the MT density and stability in control and $G\alpha o^{F/F}$;

293    $Pdx1^{Cre}$ β cells via immunofluorescence. No differences in MT density (stained for

294   tubulin) were observed between control and $G\alpha o^{-/-}$ β cells when examined in single

295   cells (Figure 5A, C) or whole islets (Figure 5B, D), as measured by the average

296   distances between MT filaments (Figure 5E). Similarly, we did not observe

297   significant differences in MT-stability in $G\alpha o^{F/F}$; $Pdx1^{Cre}$ and control β cells when the

298   levels of Glu-tubulin [a well-established marker for MT stability, resulting from the

299   removal of the C-terminal tyrosine in α tubulin to expose the glutamate residue

300   (59)] were compared (Figure 5F-H). These findings suggest that inactivating Gαo

301   does not alter MT dynamics in β cells, although both regulate IG docking and release.

302

303

304   **Fig. 5. Inactivating *Gαo* does not alter MT dynamics in β cells.** (A-E) The MT
305   density in control and $G\alpha o^{F/F}$; $Pdx1^{Cre}$ β cells, stained with anti-tubulin (green), anti-
306   insulin (red), and anti-E-cadherin (blue) antibodies. Single cells attacehd to
307   coverslips (A, C) or intact islets (B, D) were used. Insets in A, C, insulin staining to
308   identify β-cells. Note that in (B, D), a single α-tubulin and a composite channel are
309   presetented. The quantification data in E is MT density in single β cells, assayed as in
310   (35). (F-H) The density of Glu-tubulin in control and $G\alpha o^{F/F}$; $Pdx1^{Cre}$ β cells. Anti-Glu-
311   tubulin (green), E-Cadherin (red), and DAPI (blue) were used. Presented data in E
312   and H are (mean + SEM). P values, results from two-tail type II t-test. Scale bars, 5
313   µm.

314

315   In summary, we revealed two factors that act in parallel to regulate the

316   preferential secretion of newly synthesized IGs in islet β cells. One is the MT, which

317   originates from the Golgi and forms a non-directional meshwork. These properties

318   makes these MTs ideal tracks for MT-dependent transport of newly produced IGs

319   out of the trans-Golgi surface (40). However, they are unsuitable for directional bulk

320   flow of IGs (35). As a result, the MTs act as holding places for IGs in the RP, whose

13

321   transition to the RRP was expedited by both kinesin and dynein motor proteins (36,

322   38, 39). This mechanism is advantageous in that it prevents insulin over-secretion.

323   However, when IGs age and lose their association with MTs, they will no longer be

324   useful for function in the presence of a dense mesh of MTs and therefore must be

325   degraded. This poises extra stress for β cells to replace this stock via insulin

326   biosynthesis (67, 68). Note that although the absence of MTs can improve the usage

327   of the old vesicles, β cells without MTs cannot maintain long-term function, due to

328   the essential roles of MTs in β cells for new insulin biosynthesis (40).

329

330   The other factor that reduces the probability of secretion of old IGs is Gαo,

331   whose inactivation enhances GSIS by increasing IG release of relatively older IGs as

332   with MT-destabilization (15). Yet, Gαo does not regulate the MT stability or density

333   in β cells as predicted based on *in vitro* biochemical studies (69, 70). An interesting

334   future investigation could be to test if Gαo can regulate the affinity/processivity of

335   motor proteins along the MTs. It would also be worthy to examine if Gαo regulates

336   the affinity between IG and PM components that form the SNARE complex. The

337   latter possibility is particularly attractive because Gαo has been shown to interact

338   with Syntaxins (71), limiting factors for IG docking in β cells (52).

339

340   **Research Design and Methods**

341   **Mice**

342   Mouse usage followed protocols approved by the Vanderbilt University

343   IACUC for GG/IK. Mice were euthanized by isoflurane inhalation. Wild type CD-1

14

344   (ICR) mice were from Charles River (Wilmington, MA). Production of Gαo$^{F/F}$ and

345   *Pdx1^{Cre}* mice were described in (15), which were used to produce Gαo$^{-/-}$ mutant β

346   cells (*Gαo$^{F/F}$; Pdx1^{Cre}*).

347

Islet isolation and routine GSIS

349   Islets were isolated from 8-16 week-old mice using collagenase perfusion as

350   in (26). Briefly, ~2ml of 0.5 mg/mL of collagenase IV (Sigma, St. Louis, MI) dissolved

351   in Hank's Balanced Salt Solution (Corning, Corning, NY) was injected into the

352   pancreas through the main duct. The pancreas was digested at 37°C for 20 minutes

353   and washed 4 times with [RPMI-1640 media with 5.6 mM glucose (Gibco, Dublin,

354   Ireland) + 10% heat inactivated (HI) fetal bovine serum (FBS, Atlanta Biologicals,

355   Flowery Branch, GA)]. Islets were handpicked in the same media and let recover at

356   37 °C for at least 2 hours before down-stream experimentation.

357

358   GSIS follows routine procedures. Briefly, islets were washed twice with basal

359   KRB solution (111 mM NaCl, 4.8 mM KC, 1.2 mM MgSO$_4$, 1.2 mM KH$_2$PO^4, 25 mM

360   NaHCO$_3$, 10 mM HEPES, 2.8 mM glucose, 2.3 mM CaCl$_2$, and 0.2% BSA). Islets were

361   then incubated in the same solution (37 °C) for one hour, changed to new KRB to

362   start the secretion assay. For insulin secretion induction, glucose (0.5 M) and/or KCl

363   (1M) stock solutions were directly added to the KRB to desired concentrations. The

364   secretion period assayed lasts 45 minutes. After secretion, islets were immediately

365   frozen-thawed twice between -80 °C and room temperature. Acid alcohol extraction

366   (70% alcohol + 0.2% HCl) was then performed at 4 °C overnight to determine the

15

367   total insulin content. For each GSIS assays, 8-15 islets were used in 1 ml KRB. The

368   insulin levels were then assayed using an ultrasensitive Insulin Elisa kit from Alpco

369   after dilution to within the range of sensitivity.

370

371   **Islet pretreatment – MT destabilization, protein synthesis inhibition, and**

372   **radiolabeling**

373

374   For NOC treatment, islets were pre-incubated in KRB with 10 μg/ml NOC

375   (with 20 mg/ml stock in DMSO) for one-hour to depolymerize MTs. This level of

376   NOC was included in all solutions afterwards. DMSO (<0.05%) treated islets were

377   used as controls.

378

379   To inhibit protein translation, islets were incubated in RPMI-640 with 10 mM

380   glucose and 10 μM CHX for three hours to minimize the reduction of other proteins

381   that are essential for secretion (63). Secretion assays follow as above in amino acid-

382   free KRB for followup assays.

383

384   For radio-labeling, isolated islets were incubated for 12 hours in RPMI-1640

385   [supplemented with 10% FBS, 10 mM glucose, and 1/30 volume of ^{3}H-labeled

386   leucine/isoleucine (#NET1166001MC, Perkin Elmer)] cultured at 37°C with 5% CO_2.

387   Islets were then washed three times and chased in the same media without

388   radioactive amino acids for 2 hours. GSIS assays were then performed as described

389   above. In this case, the insulin levels were quantified using an Elisa kit. The

16

390   radioactivity in secreted insulin was quantified using a scintillation counter

391   (Beckman LS System 6000TA) following immunoprecipitation using guinea pig anti-

392   insulin and Protein-A beads (ThermoFisher).

393

394   **Transmission electron microscopy (TEM) detection of IG-docking**

395   Islets were incubated in RPMI-1640 with 10% FBS plus 5.6 or 20 mM glucose

396   with or without 10 μg/ml NOC for 12 hours. Islets were then fixed, sectioned, and

397   imaged following routine TEM protocols as detailed in (13). To count the number of

398   docked IGs, Image J was used to measure the length of β-cell membrane. The docked

399   vesicles, with near direct contact with the PMs (<10 nm away) were counted. The IG

400   density was counted in a similar fashion, except that β-cell cytoplasmic areas were

401   selected and measured. Double-blind tests were used without identifying the

402   treatment conditions first.

403

404   **Immunofluorescence (IF) and microscopy**

405   For Gαo staining, routine frozen pancreatic sections were used (26). Briefly,

406   adult pancreata from mice of desired genotype were dissected and fixed at 4 °C

407   overnight in 4% paraformaldehyde. Tissues were washed in PBS three-times and

408   prepared as frozen sections, followed by immunofluorescence staining using mouse

409   anti-Gαo described in (15). Insulin co-staining was used to identify β-cells. DAPI co-

410   staining was used to locate nuclei.

411

17

412   For insulin, E-cadherin, and tubulin staining, single cells or islets were used

413   as shown in (13). For single cells, islets were partially dissociated with trypsin,

414   washed, overlaid onto human fibronectin-coated coverslips, and cultured overnight

415   in RMPI-1640 media with FBS and 5.6 or 20 mM glucose. IF staining was then

416   performed according to the following: cells or islets were extracted with methanol

417   at -20°C for 5 minutes to remove free tubulin, followed by fixation with 4%

418   paraformaldehyde (PFA) for 1 (for single cells) – 4 (for islets) hours, routine

419   permeabilization and staining (13). The primary antibodies used were: rabbit anti-

420   α-Tubulin (Abcam, Cambridge, UK, #ab18251), purified mouse anti-E-Cadherin (BD,

421   San Jose, CA, #610181), rabbit anti-Glu-tubulin (MilliporeSigma #AB3201), and

422   guinea pig anti-insulin (Dako, Santa Clara, CA, #A0564). The mouse anti-Gαo

423   antibody was described in (15). Secondary antibodies are from Jackson

424   ImmunoResearch (Alexa Fluor® 647 AffiniPure Donkey Anti-Guinea Pig IgG (H+L)

425   (706-605-148); Alexa Fluor® 488 AffiniPure Donkey Anti-Rabbit IgG (H+L) (711-

426   545-152), and Alexa Fluor® 594 AffiniPure Donkey Anti-Mouse (705-585-003).

427   The dilution of all antibodies is 1:1000. Z-stacked images were captured using Nikon

428   Eclipse A1R laser scanning confocal microscope. For super-resolution, images were

429   captured at 0.125 μm intervals with DeltaVision OMX SIM Imaging System (GE

430   technology) using a 60x NA1.4 lens and processed according to the manufacturer's

431   instruction.

432

433   **IG and MT density quantification**

434   To quantify the IG localization in β cells (Figure 1), representative confocal

435   images were taken. A line-scan was then performed along the long-axis in the image

436   to quantify the IF intensity from one point in a β-cell border to another point at the

437   opposite border. The length of the line was set arbitrarily at 10 and the intensity of

438   the IF was measured using Image J. For this purpose, the lines were drawn to avoid

439   the nuclei, which are devoid of insulin IF.

440

441   MT density quantification using Image J follows the procedure described in

442   (35). Briefly, super-resolution MT images were captured as above at multiple z-

443   depth. Line scans were then used to detect the size of the spaces between MTs by

444   selecting 10 lines across the cell center with a 30-degree interval. A custom image J

445   macro was used to create line selections and obtain the intensity profile. The lengths

446   of regions without signal within the intensity profile were considered spaces

447   between MTs, with the means and SEM presented.

448

449 **Statistics**

450   For all studies, at least two biological repeats and two technical repeats were

451   included. Student t-test, two-tailed type II analysis, was used for comparisons

452   between two groups of data. Two-way ANOVA with Holm-Sidak's multiple

453   comparisons were used when more than two groups of data were compared. A p

454   value below 0.05 was considered significant.

455

456 **Resource Availability**

457

458   The reagents generated during the current studies are available from the

459   corresponding authors upon reasonable request.

460

461   **Author Contributions**

462   I.K. and G.G. conceptualized the work and designed the study. G.G. also

463   performed radiolabeling and immunoprecipitation. R.H. performed GSIS assays. R.

464   H., X.Z., and K.H. to perform immunoassays, imaging, and quantification. M. Y. did

465   vesicle quantification. All authors contributed to writing the manuscript.

466

467   **Conflict of Interest**

468   The authors declare no conflict of interest.

469

478

References

1. Swisa A, Glaser B, Dor Y. Metabolic Stress and Compromised Identity of Pancreatic Beta Cells. Front Genet. 2017;8:21.

2. Accili D, Talchai SC, Kim-Muller JY, Cinti F, Ishida E, Ordelheide AM, et al. When beta-cells fail: lessons from dedifferentiation. Diabetes Obes Metab. 2016;18 Suppl 1:117-22.

3. Alejandro EU, Gregg B, Blandino-Rosano M, Cras-Meneur C, Bernal-Mizrachi E. Natural history of beta-cell adaptation and failure in type 2 diabetes. Mol Aspects Med. 2015;42:19-41.

4. Maiese K, Morhan SD, Chong ZZ. Oxidative stress biology and cell injury during type 1 and type 2 diabetes Mellitus. Curr Neurovasc Res. 2007;4(1):63-71.

5. Guettier J, Gorden P. Insulin secretion and insulin-producing tumors. Expert Rev Endocrinol Metab. 2010(5):217-27.

6. Nessa A, Rahman SA, Hussain K. Molecular mechanisms of congenital hyperinsulinism and prospective therapeutic targets. Expert Opin Orphan D. 2015;3(8):887-98.

7. Rahman SA, Nessa A, Hussain K. Molecular mechanisms of congenital hyperinsulinism. J Mol Endocrinol. 2015;54(2):R119-R29.

8. Hou JCQ, Min L, Pessin JE. Insulin Granule Biogenesis, Trafficking and Exocytosis. Vitam Horm. 2009;80:473-506.

9. Olofsson CS, Gopel SO, Barg S, Galvanovskis J, Ma XS, Salehi A, et al. Fast insulin secretion reflects exocytosis of docked granules in mouse pancreatic B-cells. Pflug Arch Eur J Phy. 2002;444(1-2):43-51.

10. Rorsman P, Renstrom E. Insulin granule dynamics in pancreatic beta cells. Diabetologia. 2003;46(8):1029-45.

11. Daniel S, Noda M, Straub SG, Sharp GWG. Identification of the docked granule pool responsible for the first phase of glucose-stimulated insulin secretion. Diabetes. 1999;48(9):1686-90.

12. Del Prato S, Tiengo A. The importance of first-phase insulin secretion: implications for the therapy of type 2 diabetes mellitus. Diabetes-Metab Res. 2001;17(3):164-74.

13. Huang C, Walker EM, Dadi PK, Hu R, Xu Y, Zhang W, et al. Synaptotagmin 4 Regulates Pancreatic beta Cell Maturation by Modulating the Ca(2+) Sensitivity of Insulin Secretion Vesicles. Dev Cell. 2018;45(3):347-61 e5.

14. Ohara-Imaizumi M, Nakamichi Y, Tanaka T, Ishida H, Nagamatsu S. Imaging exocytosis of single insulin secretory granules with evanescent wave microscopy - Distinct behavior of granule motion in biphasic insulin release. Journal of Biological Chemistry. 2002;277(6):3805-8.

15. Zhao A, Ohara-Imaizumi M, Brissova M, Benninger RK, Xu Y, Hao Y, et al. Galphao represses insulin secretion by reducing vesicular docking in pancreatic beta-cells. Diabetes. 2010;59(10):2522-9.

16. Hao MM, Li X, Rizzo MA, Rocheleau JV, Dawant BM, Piston DW. Regulation of two insulin granule populations within the reserve pool by distinct calcium sources. J Cell Sci. 2005;118(24):5873-84.

525   17.   Gandasi NR, Yin P, Omar-Hmeadi M, Ottosson Laakso E, Vikman P, Barg S.
526   Glucose-Dependent Granule Docking Limits Insulin Secretion and Is Decreased in
527   Human Type 2 Diabetes. Cell Metab. 2018;27(2):470-8 e4.
528   18.   Rhodes CJ, Halban PA. Newly synthesized proinsulin/insulin and stored
529   insulin are released from pancreatic B cells predominantly via a regulated, rather
530   than a constitutive, pathway. J Cell Biol. 1987;105(1):145-53.
531   19.   Hou N, Mogami H, Kubota-Murata C, Sun M, Takeuchi T, Torii S. Preferential
532   release of newly synthesized insulin assessed by a multi-label reporter system using
533   pancreatic beta-cell line MIN6. PLoS One. 2012;7(10):e47921.
534   20.   Halban PA. Differential rates of release of newly synthesized and of stored
535   insulin from pancreatic islets. Endocrinology. 1982;110(4):1183-8.
536   21.   Gold G, Gishizky ML, Grodsky GM. Evidence that glucose "marks" beta cells
537   resulting in preferential release of newly synthesized insulin. Science.
538   1982;218(4567):56-8.
539   22.   Georgiadou E, Rutter GA. Age matters: Grading granule secretion in beta cells.
540   J Biol Chem. 2020;295(27):8912-3.
541   23.   Yau B, Hays L, Liang C, Laybutt DR, Thomas HE, Gunton JE, et al. A fluorescent
542   timer reporter enables sorting of insulin secretory granules by age. Journal of
543   Biological Chemistry. 2020;295(27):8901-11.
544   24.   Marsh BJ, Soden C, Alarcon C, Wicksteed BL, Yaekura K, Costin AJ, et al.
545   Regulated autophagy controls hormone content in secretory-deficient pancreatic
546   endocrine beta-cells. Mol Endocrinol. 2007;21(9):2255-69.
547   25.   Halban PA, Wollheim CB. Intracellular Degradation of Insulin Stores by Rat
548   Pancreatic-Islets Invitro - an Alternative Pathway for Homeostasis of Pancreatic
549   Insulin Content. Journal of Biological Chemistry. 1980;255(13):6003-6.
550   26.   Hu R, Walker E, Huang C, Y. X, Weng C, Erickson GE, et al. Myt Transcription
551   Factors prevent stress-response gene overactivation to enable postnatal pancreatic
552   β-cell proliferation, function, and survival. Dev Cell. 2020;In press.
553   27.   Szabat M, Page MM, Panzhinskiy E, Skovso S, Mojibian M, Fernandez-Tajes J,
554   et al. Reduced Insulin Production Relieves Endoplasmic Reticulum Stress and
555   Induces beta Cell Proliferation. Cell Metab. 2016;23(1):179-93.
556   28.   Yong J, Itkin-Ansari P, Kaufman RJ. When Less Is Better: ER Stress and Beta
557   Cell Proliferation. Dev Cell. 2016;36(1):4-6.
558   29.   Sharma RB, O'Donnell AC, Stamateris RE, Ha B, McCloskey KM, Reynolds PR,
559   et al. Insulin demand regulates beta cell number via the unfolded protein response. J
560   Clin Invest. 2015;125(10):3831-46.
561   30.   Hoboth P, Muller A, Ivanova A, Mziaut H, Dehghany J, Sonmez A, et al. Aged
562   insulin granules display reduced microtubule-dependent mobility and are disposed
563   within actin-positive multigranular bodies. Proc Natl Acad Sci U S A.
564   2015;112(7):E667-76.
565   31.   Brouhard GJ, Rice LM. Microtubule dynamics: an interplay of biochemistry
566   and mechanics. Nat Rev Mol Cell Bio. 2018;19(7):451-63.
567   32.   Mallik R, Rai AK, Barak P, Rai A, Kunwar A. Teamwork in microtubule motors.
568   Trends Cell Biol. 2013;23(11):575-82.

569   33.   Franker MAM, Hoogenraad CC. Microtubule-based transport - basic
570   mechanisms, traffic rules and role in neurological pathogenesis. J Cell Sci.
571   2013;126(11):2319-29.
572   34.   Bracey KM, Ho KH, Yampolsky D, Gu G, Kaverina I, Holmes WR. Microtubules
573   Regulate Localization and Availability of Insulin Granules in Pancreatic Beta Cells.
574   Biophys J. 2020;118(1):193-206.
575   35.   Zhu X, Hu R, Brissova M, Stein RW, Powers AC, Gu G, et al. Microtubules
576   Negatively Regulate Insulin Secretion in Pancreatic beta Cells. Dev Cell.
577   2015;34(6):656-68.
578   36.   Varadi A, Ainscow EK, Allan VJ, Rutter GA. Involvement of conventional
579   kinesin in glucose-stimulated secretory granule movements and exocytosis in clonal
580   pancreatic beta-cells. J Cell Sci. 2002;115(21):4177-89.
581   37.   Wang ZX, Thurmond DC. Mechanisms of biphasic insulin-granule exocytosis -
582   roles of the cytoskeleton, small GTPases and SNARE proteins. J Cell Sci.
583   2009;122(7):893-903.
584   38.   Cui J, Wang Z, Cheng QN, Lin RZ, Zhang XM, Leung PS, et al. Targeted
585   Inactivation of Kinesin-1 in Pancreatic beta-Cells In Vivo Leads to Insulin Secretory
586   Deficiency. Diabetes. 2011;60(1):320-30.
587   39.   McDonald A, Fogarty S, Leclerc I, Hill EV, Hardie DG, Rutter GA. Control of
588   insulin granule dynamics by AMPK dependent KLC1 phosphorylation. Islets.
589   2009;1(3):198-209.
590   40.   Trogden KP, Zhu X, Lee JS, Wright CVE, Gu G, Kaverina I. Regulation of
591   Glucose-Dependent Golgi-Derived Microtubules by cAMP/EPAC2 Promotes
592   Secretory Vesicle Biogenesis in Pancreatic beta Cells. Curr Biol. 2019;29(14):2339-
593   50 e5.
594   41.   Howell SL, Hii CS, Shaikh S, Tyhurst M. Effects of Taxol and Nocodazole on
595   Insulin-Secretion from Isolated Rat Islets of Langerhans. Bioscience Rep.
596   1982;2(10):795-801.
597   42.   Kasai K, Fujita T, Gomi H, Izumi T. Docking is not a prerequisite but a
598   temporal constraint for fusion of secretory granules. Traffic. 2008;9(7):1191-203.
599   43.   Yasuda T, Shibasaki T, Minami K, Takahashi H, Mizoguchi A, Uriu Y, et al.
600   Rim2 alpha Determines Docking and Priming States in Insulin Granule Exocytosis.
601   Cell Metabolism. 2010;12(2):117-29.
602   44.   Gaisano HY. Recent new insights into the role of SNARE and associated
603   proteins in insulin granule exocytosis. Diabetes Obesity & Metabolism. 2017;19:115-
604   23.
605   45.   Sudhof TC. Synaptotagmins: why so many? J Biol Chem. 2002;277(10):7629-
606   32.
607   46.   Tucker WC, Chapman ER. Role of synaptotagmin in Ca2+-triggered
608   exocytosis. Biochem J. 2002;366(Pt 1):1-13.
609   47.   Groffen AJ. Doc2b is a high-affinity Ca2+ sensor for spontaneous
610   neurotransmitter release (vol 327, pg 1614, 2010). Science. 2010;328(5979):690-.
611   48.   Houy S, Groffen AJ, Ziomkiewicz I, Verhage M, Pinheiro PS, Sorensen JB.
612   Doc2B acts as a calcium sensor for vesicle priming requiring synaptotagmin-1,
613   Munc13-2 and SNAREs. Elife. 2017;6.

614   49.   Ramalingam L, Oh E, Yoder SM, Brozinick JT, Kalwat MA, Groffen AJ, et al.
615   Doc2b Is a Key Effector of Insulin Secretion and Skeletal Muscle Insulin Sensitivity.
616   Diabetes. 2012;61(10):2424-32.
617   50.   Sudhof TC. A molecular machine for neurotransmitter release:
618   synaptotagmin and beyond. Nat Med. 2013;19(10):1227-31.
619   51.   Xie L, Zhu D, Dolai S, Liang T, Qin TR, Kang YH, et al. Syntaxin-4 mediates
620   exocytosis of pre-docked and newcomer insulin granules underlying biphasic
621   glucose-stimulated insulin secretion in human pancreatic beta cells. Diabetologia.
622   2015;58(6):1250-9.
623   52.   Oh E, Miller RA, Thurmond DC. Syntaxin 4 Overexpression Ameliorates
624   Effects of Aging and High-Fat Diet on Glucose Control and Extends Lifespan. Cell
625   Metabolism. 2015;22(3):499-507.
626   53.   Liang T, Qin TR, Xie L, Dolai S, Zhu D, Prentice KJ, et al. New Roles of Syntaxin-
627   1A in Insulin Granule Exocytosis and Replenishment. Journal of Biological
628   Chemistry. 2017;292(6):2203-16.
629   54.   Jewell JL, Oh E, Thurmond DC. Exocytosis mechanisms underlying insulin
630   release and glucose uptake: conserved roles for Munc18c and syntaxin 4. Am J
631   Physiol-Reg I. 2010;298(3):R517-R31.
632   55.   Oldham WM, Hamm HE. Heterotrimeric G protein activation by G-protein-
633   coupled receptors. Nat Rev Mol Cell Bio. 2008;9(1):60-71.
634   56.   El-Armouche A, Zolk O, Rau T, Eschenhagen T. Inhibitory G-proteins and their
635   role in desensitization of the adenylyl cyclase pathway in heart failure. Cardiovasc
636   Res. 2003;60(3):478-87.
637   57.   Roychowdhury S, Panda D, Wilson L, Rasenick MM. G protein alpha subunits
638   activate tubulin GTPase and modulate microtubule polymerization dynamics. J Biol
639   Chem. 1999;274(19):13485-90.
640   58.   Tabei SMA, Burov S, Kim HY, Kuznetsov A, Huynh T, Jureller J, et al.
641   Intracellular transport of insulin granules is a subordinated random walk. P Natl
642   Acad Sci USA. 2013;110(13):4911-6.
643   59.   Ho KH, Yang XD, Osipovich AB, Cabrera O, Hayashi ML, Magnuson MA, et al.
644   Glucose Regulates Microtubule Disassembly and the Dose of Insulin Secretion via
645   Tau Phosphorylation. Diabetes. 2020;69(9):1936-47.
646   60.   Heaslip AT, Nelson SR, Lombardo AT, Previs SB, Armstrong J, Warshaw DM.
647   Cytoskeletal Dependence of Insulin Granule Movement Dynamics in INS-1 Beta-Cells
648   in Response to Glucose. Plos One. 2014;9(10).
649   61.   Donelan MJ, Morfini G, Julyan R, Sommers S, Hays L, Kajio H, et al. Ca2+-
650   dependent dephosphorylation of kinesin heavy chain on beta-granules in pancreatic
651   beta-cells - Implications for regulated beta-granule transport and insulin exocytosis.
652   Journal of Biological Chemistry. 2002;277(27):24232-42.
653   62.   Ivarsson R, Obermuller S, Rutter GA, Galvanovskis J, Renstrom E.
654   Temperature-sensitive random insulin granule diffusion is a prerequisite for
655   recruiting granules for release. Traffic. 2004;5(10):750-62.
656   63.   Garcia-Barrado MJ, Ravier MA, Rolland JF, Gilon P, Nenquin M, Henquin JC.
657   Inhibition of protein synthesis sequentially impairs distinct steps of stimulus-
658   secretion coupling in pancreatic beta cells. Endocrinology. 2001;142(1):299-307.

659 64.   Howell SL, Taylor KW. Secretion of Newly Synthesized Insulin in Vitro.
660   Biochemical Journal. 1967;102(3):922-&.
661 65.   Roychowdhury S, Rasenick MM. Submembraneous microtubule cytoskeleton:
662   regulation of microtubule assembly by heterotrimeric Gproteins. FEBS J.
663   2008;275(19):4654-63.
664 66.   Roychowdhury S, Rasenick MM. G protein beta 1 gamma 2 subunits promote
665   microtubule assembly. Journal of Biological Chemistry. 1997;272(50):31576-81.
666 67.   Cao SS, Kaufman RJ. Endoplasmic reticulum stress and oxidative stress in cell
667   fate decision and human disease. Antioxid Redox Signal. 2014;21(3):396-413.
668 68.   Wang M, Kaufman RJ. Protein misfolding in the endoplasmic reticulum as a
669   conduit to human disease. Nature. 2016;529(7586):326-35.
670 69.   Roychowdhury S, Martinez L, Salgado L, Das S, Rasenick MM. G protein
671   activation is prerequisite for functional coupling between Galpha/Gbetagamma and
672   tubulin/microtubules. Biochem Biophys Res Commun. 2006;340(2):441-8.
673 70.   Schappi JM, Krbanjevic A, Rasenick MM. Tubulin, actin and heterotrimeric G
674   proteins: coordination of signaling and structure. Biochim Biophys Acta.
675   2014;1838(2):674-81.
676 71.   Li Q, Lau A, Morris TJ, Guo L, Fordyce CB, Stanley EF. A syntaxin 1, G alpha(o),
677   and N-type calcium channel complex at a presynaptic nerve terminal: Analysis by
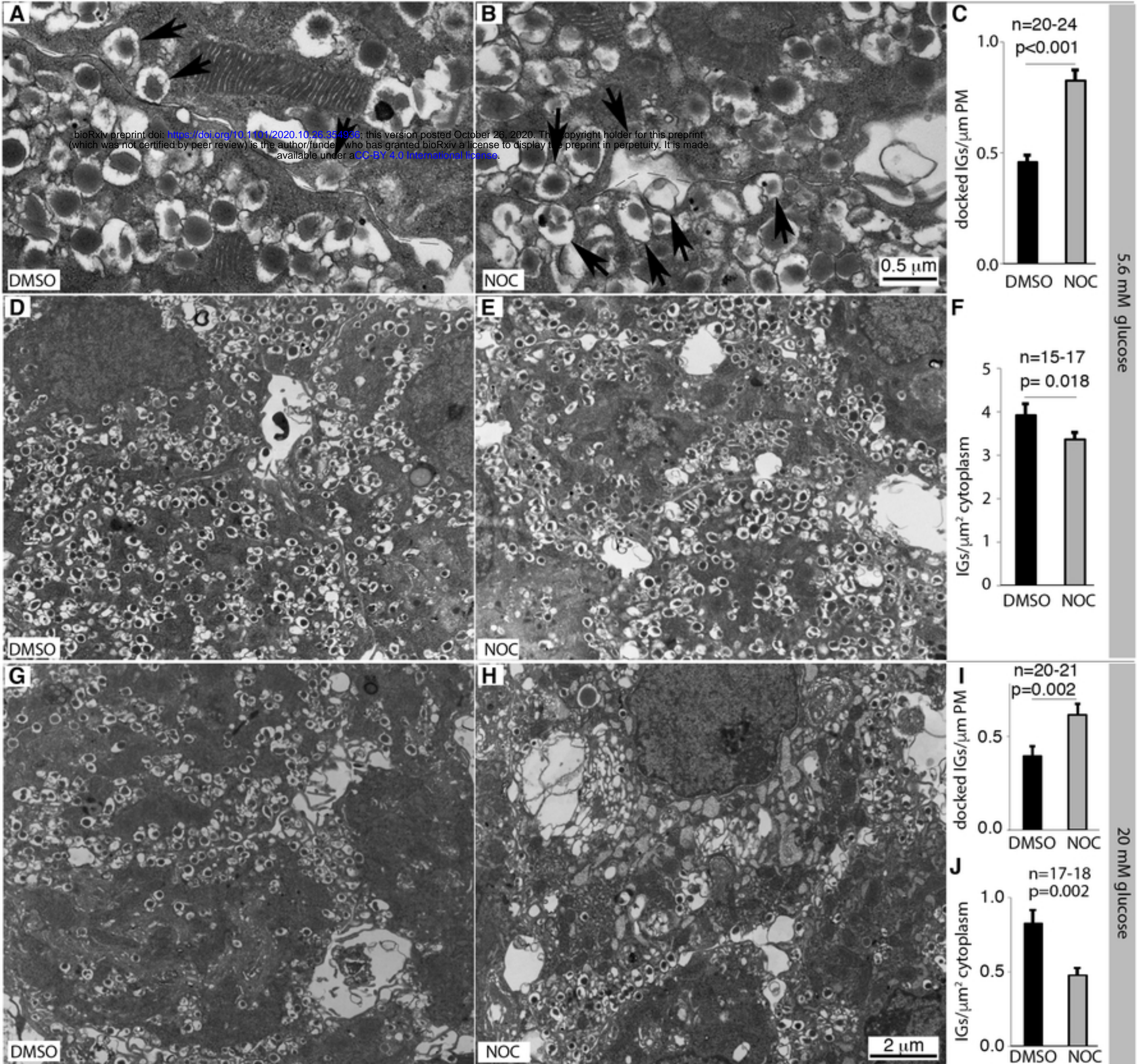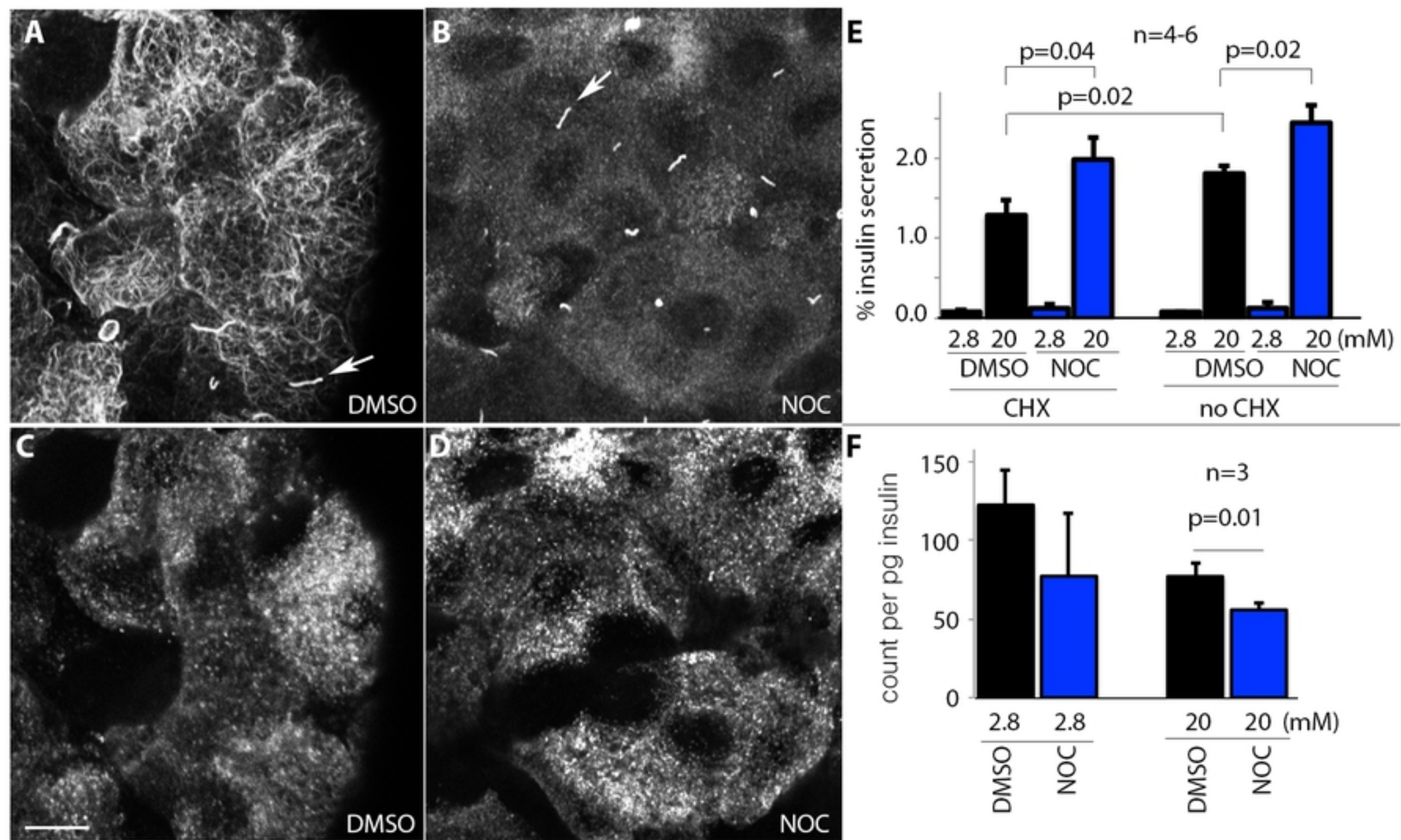678   quantitative immunocolocalization. J Neurosci. 2004;24(16):4070-81.
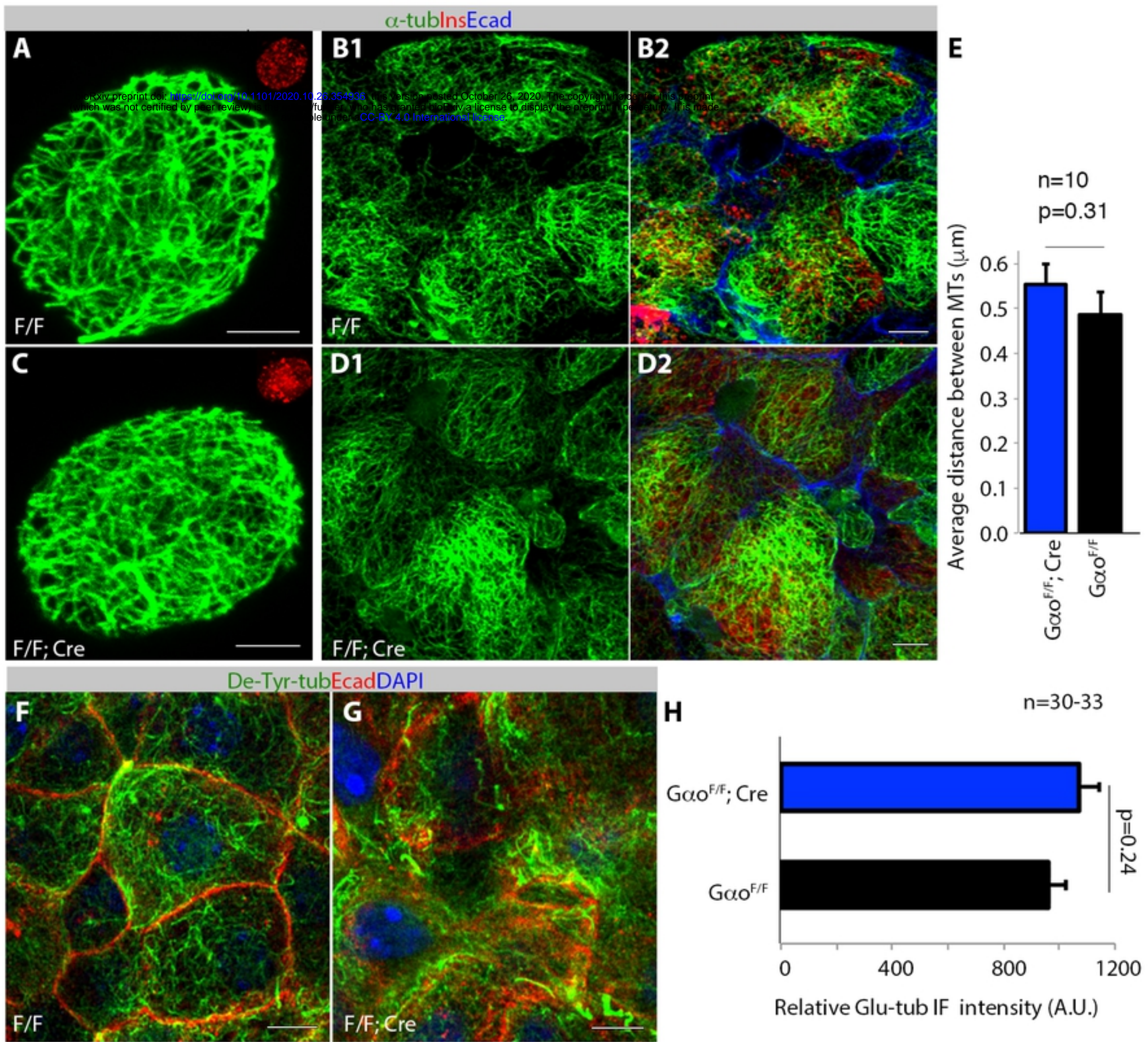679

Figure 2

Figure 3

α-tubInsEcad

De-Tyr-tubEcadDAPI

Figure 5

Figure 1

Figure 4